Polymer-free gel electrolyte and its application in TiO2 -based electrochromic devices

H. M.B.I. Gunathilaka
University of Peradeniya
V. A. Seneviratne
University of Peradeniya
H. N.M. Sarangika (✉ sarangikah@appsc.sab.ac.lk)
Sabaragamuwa University of Sri Lanka

Research Article

Keywords: Electrochromic Device, Polymer-free gel electrolyte, Ionic Conductivity, Optical Modulation, Switching speed

Posted Date: January 31st, 2023

DOI: https://doi.org/10.21203/rs.3.rs-2524497/v1

Additional Declarations: No competing interests reported.

Version of Record: A version of this preprint was published at Journal of Applied Electrochemistry on May 19th, 2023. See the published version at https://doi.org/10.1007/s10800-023-01912-0.

Abstract

Electrochromic devices based on polymer-free gel electrolytes (PFGE), offer several advantages over polymer electrolytes. The preparation and characterization of a fumed silica-based PFGE and its applications in TiO_2 electrochromic devices (ECD) were the main aims of the present study. A series of liquid electrolytes were prepared by mixing lithium chloride (LiCl) and ethylene Glycol (EG). The total oxygen moles of EG to lithium ions of LiCl ratio (O: Li^+) was altered from 5:1 to 80:1 and the ionic conductivities were measured. The highest ionic conductivity was observed for 15: 1 molar ratio with the value being the 1.28×10^{-2} S cm^{-1}.

In order to prepare PFGE, (10 wt. %) of fumed silica from the total weight of EG and LiCl were added to the optimized liquid electrolyte EG/LiCl as the polymer-free gelling agent. The maximum ionic conductivity was found in O: Li = 10: 1, with the value being 8.94×10^{-3} S cm^{-1}. Notable electrochromic properties of TiO_2/FTO were observed with higher optical modulation of 73% at 700 nm and a noticeable switching speed of $T_{bleaching}$= 42.5 s and $T_{coloring}$= 16.7 s were observed.

1. Introduction

The expanding crisis of energy and environmental challenges feels a necessity for the evolution of sustainable, economical and renewable resources. Electrochromism is referred to as unique characteristic of materials in which optical properties being vary their color state reversibly when subjected to a small electric field. In recent two decades, electronics has taken much more attention regarding low power consumption in daily life routine. For the technology of smart windows, electrochromism, thermochromism, and photochromism are effective energy conservation techniques which control lighting and temperature [1–3]. ECDs are widely used in promising applications such as buildings, displays, windows, sunroofs, and agricultural lighting controllers to control and maintain incoming light and heat.

Electrochromism is one of the best experiences for the color changes in a redox reaction of Electrochromic materials (ECMs) and active ions. An ECD mainly be made up of three main components such as an active electrode, an electrolyte, and a counter electrode. ECMs are mostly organic or inorganic compounds [4]. The optical properties such as transmittance, absorption, and reflectance can be changed due to changes in the electronic state of complex molecules. This change in the electronic state of the molecule is a reversible process and it can be happened by applying sufficient voltage. It results in the absorption of a range of electromagnetic radiation of different visible colors when switching between redox states.[5, 6]. Cation (M^+) insertion to the ECM is the common type and electronic stability is balanced by the absorption of a balancing electron. This can be illustrated in the following stoichiometric equation [7].

$$\mathrm{ECM} + \mathrm{xe}^- + \mathrm{xM}^+ \leftrightarrow \mathrm{M_xECM} \quad [1]$$

Normally, oxide-based ECDs have two types of electrochromic films, and they are named as cathodic oxide (e.g., W, Mo, Ti and Nb) and anodic oxide (e.g., Ni and Ir) [8–13].

Although lots of materials show electrochromic properties, quite all of them are not commercialized and out of them, tungsten oxide (WO_3) has been the most deeply studied ECM used in ECDs[14–16]. However, the electrochromic properties and coloration cycle of WO_3 strongly depend on its preparation techniques and structure. Vacuum evaporation and sputtering technique are given high coloring performances in WO_3 thin films.

However, these methods are difficult to apply in large-area commercial applications since they are expensive and time-consuming. Among other ECMs, TiO_2 might be a possible substitution for tungsten trioxide owing to its inherent advantages such as low cost, abundance, and low environmental impact. In early studies, transparent films were also fabricated using processed TiO_2 applying simple techniques such as doctor blading [17], screen printing [18], spraying [19] etc.

Apart from the active electrode, another critical component is an electrolyte. It is crucial for the improvement of the efficiency and stability of ECDs due to the ionic movements through it. Liquid-type electrolytes are more common in efficient ECDs and their pragmatic applications are bounded due to some technical issues, such as durability, leakage, and relatively low long-term stability related with other chemical constituents and the presence of water and volatile solvents. Therefore, considerable interest is raised in solid-state or quasi-solid-state electrolytes for ECDs.

In spite of the advantages of gel electrolytes, quiet there are a few drawbacks such as low ionic conductivity and relatively small cycle life. Generally, crystalline polymers are not suitable for batteries and ECDs due to their low conductivity [20]. In solvent-doped polymer electrolytes systems have overcome promising properties such as volatilization, electrode corrosion, and the absence of leakage for ECDs. Although organic polymer electrolytes are widely used in ECDs, several limitations such as cycle life and flammability have been monitored[21][22].

Fumed silica has been used as a substitution for the gelling medium. It is concerned as a high-surface molecule in surface chemistry. In an aprotic solvent, hydroxyl groups can interact with silica via hydrogen bonding of the surface, which results in the formation of a three-dimensional structure. In composite polymer electrolytes (CPEs), fumed silica isn't used as a catalyst like ethylene carbonate, while it is used as a catalyst supporter instead. The properties of carbon and silicon are almost different if silicon is below to carbon in the same group. Because Si-O linkages with polymers are important due to thermal stability, chemical stability, and oxidative stability.

There are a lot of studies have been done addressing SiO_2 and TiO_2 nanoparticles with polymer matrix as a filler by enriching the amorphous nature of the gel polymer[23, 24]. Almost all early research and experiments have been done on SiO_2 composite polymer gel electrolytes, but they did not apply merely fumed silica to the electrolyte of ECD. By considering all the aforementioned reasons, the fabrication of a

novel polymer-free gel electrolyte-based electrochromic device using TiO_2 as the electrochromic material with FTO as the counter electrode and a mixture of EG/LiCl/Fumed silica as the ion-conducting electrolyte was focused.

2. Experimental

2.1 Materials

In this study, highly pure chemicals and materials were used as starting materials. Ethylene glycol (EG) (anhydrous, purity ≥ 99.8%), Lithium chloride (LiCl) (purity ≥ 99.98%), fumed silica (SiO_2) (F. W. 60.09, hydroscopic, surface area 380 m^2 g^{-1}, 7 nm, Sigma Aldrich, purity > 99.8%), Titanium dioxide (TiO_2) (Sigma-Aldrich, Titania paste, transparent) were purchased.

2.2 Preparation of electrolyte

An appropriate amount of vacuum-dried LiCl was added to the EG solvent and a set of liquid electrolytes were prepared by varying the ratio of total oxygen atoms from EG molecules to a Li^+ ion from LiCl molecule (O: Li^+ = n: 1). Different weight percentages of dehydrated fumed silica (10, 12 and 15 wt. %) were introduced to the liquid electrolytes and mixtures were stirred until a clear gel was obtained. The 10 wt.% fumed silica was selected to prepare the gel electrolytes for further characterization.

2.3 Electrolyte characterization

The ionic conductivities of the liquid and the gel electrolyte were calculated applying AC complex impedance spectroscopy using Solatron SI-1260 impedance analyzer and Autolab 3 instruments in the frequency range 20 Hz – 10 MHz. The liquid electrolyte was filled into a special holder by blocking two stainless steel electrodes and the impedance was measured at room temperature. The PFGE was trapped between two stainless steel electrodes and put it into an oven to measure the AC impedance measurement with respect to different temperatures. Concerning the electrochemical performances and the stability of the liquid and the gel electrolytes, the highest conducting liquid and PFGEs were selected and characterized. They were characterized by testing cycle life and performance by changing the scan rate by using Metrohm Auto lab 2 and Bio Logic SP-300. FTIR spectrums of liquid and polymer-free gels were obtained in the range of 4000–550 cm^{-1} using Bruker tensor 27 IR spectrophotometer and the attenuated total reflectance attachment was used to obtain the spectrum for the gels and liquids. The morphology and microscopic information of the PFGEs were investigated using Scanning electron microscopy (SEM).

2.4 Fabrication of the ECD

FTO glass was coated by commercial TiO_2 paste using the “Doctor Blade” technique and it was sintered in a high-temperature furnace at 450°C. ECDs were fixed as FTO glass/TiO_2/ PFGE/FTO glass with dimensions 2.0 × 1.5 cm^2 as follows. A 0.2 mm spacer was kept on the TiO_2 electrode to maintain even

spacing for the electrical insulation from the FTO. Then the frame was filled with the PFGE and another FTO plate was put on the electrolyte layer as a counter electrode.

2.5 Electrochemical performances

Electrochemical properties of the ECD were analyzed by using cyclic voltammetry and, it was carried out using Metrohm Autolab 2 with three electrode configurations, where TiO_2 coated FTO served as the working electrode, silver /silver chloride (Ag/AgCl) electrode served as the reference electrode and carbon rod as the counter electrode. The liquid electrolyte has been tested for 500 cycles under cyclic voltammetry for different scan rates ranging from 4 mVs^{-1} to 400 mVs^{-1}.

The performance of the ECDs was tested, by applying a small voltage externally between two electrodes. The potential difference between the counter electrode and the working electrode was increased gradually from 0.0 V to 4.2 V. The transmittance of the devices was measured by Using Shimadzu UV-1800 under a range between 400–1100 nm. Transmittance at 700nm was recorded while toggling applied voltage 4.2 V and − 0.5 V to obtain the kinetic graph.

3. Results And Discussion

3.1 Ionic Conductivity

Clear transparent solutions were obtained for different compositions of EG and LiCl with O to Li ratio of n:1.(O to Li ratio is the number of Oxygen atoms from EG molecules to the no of Li atoms from LiCl) LiCl salt is highly dissolved in EG and results in highly viscous electrolytes. Conductivity variations of the liquid electrolytes at room temperature are shown in Fig. 1 as a function of n: 1 molar ratio. Results indicate that the ionic conductivity enhancement in the liquid electrolytes with the decrease of n:1 ratio from 5: 1with the highest value being the 1.28 x 10^{-2} S cm^{-1}at n: 1 = 15 :1. According to the graph, further increment in the salt concentration gradually decreases the ionic conductivity. Increment in the ionic conductivity with the Li^+ concentration is interconnected with the number of mobile ions. However, the fall in the ionic conductivity of liquid electrolyte from 15:1 to 5:1 molar ratio is due to the agglomeration of ions and the hindrance to the ionic mobility due to agglomerations[25]. This reduces the free ions in the solution and the ionic mobility[26]. If the concentration goes beyond the solubility limit of the salt in the solvent, it will separate as a precipitate and this may cause to make crystalline phase in the electrolyte. Hence resistance for ion transfer increases and ionic conductivity decreases accordingly.

[Fig. 1. about here.]

LiCl, EG, Nano-Silica polymer free gel electrolyte was prepared by adding different percentages of dehydrated fumed silica (8, 10, 12, and 15 wt. %) into the liquid electrolyte, and mixtures were stirred until a clear gel was obtained. The best gelling properties was observed for the 10 wt.% fumed silica and it was selected to prepare the gel electrolytes for further characterization. When 10 wt. % of fumed silica was added to the liquid electrolyte, the ionic conductivities of GEs of all O: Li^+ ratios were dropped

compared to the conductivities of liquid electrolytes. The reduction of the ionic conductivity in the gel form is due to hindrance to the ionic mobility in the gel medium due to increased viscosity. The ionic conductivity of the PFGEs increases with the salt concentration until O: Li^+ = 10:1 and decreases gradually when the salt concentration is increased further. Although the ionic conductivity of the liquid electrolyte was optimized at O: Li^+ =15:1, the highest conductivity for gels were obtained at O: Li^+ =10:1 with 10 wt.% fumed silica. This can be verified by calculating the pre-exponential factor and the activation energy for the PFGE and values are given in Table 1. The activation energy (E_a) of a gel electrolyte presents the properties of energy characteristics. Among the studied samples, the lowest activation energy was obtained in sample 2 which has the maximum ionic conductivity. The amount of charge carriers in the electrolyte is proportional to the pre-exponential factor and values obtained for the electrolyte composition for O: Li^+ =15:1 and O: Li^+ =7.5: 1 ratio were almost the same. This might be due to the reduced ion aggregations of electrolyte O: Li^+ = 10:1 with the addition of the fumed silica and it shows low activation energy than the O: Li^+=7.5: 1 ratio.

Table 1
Ionic conductivity values, pre-exponential factor 'A' values and activation energy Ea of the polymer free gel electrolyte

Electrolyte Sample	Ratio of the total Li^+ ion moles to O moles of the EG (n:1)	σ_{RT} $\times 10^{-3}$ (Scm^{-1}), (298K)	σ $\times 10^{-3}$ (Scm^{-1}), (333K)	A (S cm^{-1} K)	E_a(kJ mol^{-1})
1	7.5:1	3.212	0.869	40.3665	23.452
2	10:1	8.935	2.057	45.3722	21.369
3	15:1	6.706	1.508	40.1090	21.878

[Table 1 about here.]

The Nyquist plot of the gel electrolyte with O: Li^+ ratio of 10:1 at 25°C is given in Fig. 2(a). High-frequency semi-circle disappearing in the plot is due to poor electrochemical activity and the charge exchange process[27]. Figure 2(b) shows the ionic conductivity variations of studied gel electrolyte samples according to the temperature. It shows an increase in the ac conductivity with increasing temperature. This may be due to the dissociation of ion aggregates with increasing temperature. The curves obtained for the variation of ionic conductivity (σ) of the gel electrolyte systems at elevated temperatures can be well fitted with the Arrhenius equation given in Eq. 2.

$$\sigma = Aexp\left(-\frac{E_a}{kT}\right)$$

2

Where A is the Arrhenius constant (pre-exponential factor), E_a is the activation energy, and T is the absolute temperature. And k is the Boltzmann constant

[Fig. 2 about here.]

3.2 FTIR analysis

FTIR spectroscopy was analyzed to get a better understanding of binding ability among compounds, solubility, and structural behavior of EG/LiCl blends[28]. The best ionic conductive solutions of the EG/LiCl series and pure EG were systematically studied in order to determine the interaction of the Li ions with the solution. In the FTIR spectrum, particular attention on the peaks analogous to functional groups in the range of 4000 – 550 cm^{-1} [29] was mainly focused.

[Fig. 3 about here.]

Peaks inherent in 3100–3600 and 900–1200 cm^{-1} are identical to the (O-H) and (C-O) stretching modes. The peak in 3100–3600 $cm^{-1}$was corresponded to the O-H stretching mode of EG [30]. Variation of the peak intensity of C-O bonds (900–1200 cm^{-1}) with the addition of LiCl salts is shown in the Fig. 3b. However, O-H stretching vibrations decreases with the increasing Li-ion concentration as in Fig. 3a. This may be due to the hydration of Li^+. This effect causes the sudden decrease of the ionic conductivity while increasing the Li^+ ion of liquids from n:1 = 15:1 to 5:1 molar ratio. This is agreeing with the diminution of ionic conductivity with the increment of LiCl concentration beyond 15:1 molar ratio. The ion transportation characteristics are mainly affected by the ionic clusters in electrolyte systems. Ion transportation of Mg-based electrolyte has been investigated for the ionic agglomeration with the electroactive species analyzing the solvation structure and found that it was not affected by the solute concentration [31]. Li-ion agglomeration in this study is mainly due to the arrangement of ions and molecules as ion pairs and aggregates. The possible ion pair and aggregates were illustrated in Fig. 4. The presence of different ionic species could be proved by FTIR analysis if large cations have been used. The cation modes are very sensitive to what those are bonded to[32, 33]

[Fig. 4 about here.]

However, as expected, C-O-H bending vibration mode has a peak at 1405 cm^{-1}, CH_2 wagging vibrations at 1330cm^{-1} and C-O stretching vibrations at 1081 cm^{-1} have been shifted with the increase of the salt concentration due to the bathochromic shift. The rearrangement of π-electrons in alternating bonds are shorten the distance and condensed each other while increasing the salt concentration[34, 35]. Also, the intensity of the C-C stretching mode at 864 cm^{-1} has reduced with the increasing Li^+ concentration and no change in the peak position as well. It clarifies the minimum effect of Li^+ ions to the C-C bonds because the attraction of Li ions to EG molecules. This confirms the symmetric bonding of two Li to the two OH groups on the two sides of the EG molecules.

The FTIR spectra of liquid electrolyte and PFGE have almost identical peaks except mainly the Si-O bending vibrations at 801 cm^{-1} in the spectrum of PFGE and C-H stretching vibrations at 1260 cm^{-1} in the spectrum of liquid electrolyte. Owing to low interaction of fumed silica with EG is facilitating the ionic conductivity of the PFGE.

[Fig. 5 about here.]

According to Fig. 5, the C-O stretching vibration mode has shifted identically with the reducing Li^+ ion concentration in the gel electrolyte. C-O stretching mode of the pure EG at 1083 cm^{-1} has systematically shifted up to 1076 cm^{-1} from 10:1 liquid electrolyte sample to 20:1 PFGE sample. It is identified that it should be shifted right with the reducing Li^+ concentration. But it has been shifted left due to the impact of agglomeration with fumed silica. Other identified vibrational modes of liquid electrolyte and PFGE were listed in table II.

[Table 2about here.]

Table 2
Identified vibration modes in liquid electrolyte and polymer free gel electrolyte

Identified Vibration Mode	**Liquid electrolyte Wavelength (cm^{-1})**	**Polymer free gel electrolyte Wavelength (cm^{-1})**
OH stretching	3280	3274
CO stretching	1081	1076
C-C stretching	862	862
CH_2 wagging	-	1255
CH_2 wagging	1371	1367
C-O-H bending	1407	1408
CH_2 bending	1455	1457
C-H stretching sys.	2877	2877
C-H stretching asys.	2943	2943
C- H rocking	881	881

3.3 Stability of the liquid electrolyte system

Cyclic voltammetry of optimized FTO/ TiO_2, EG and LiCl liquid electrolyte from 1 to 500th cycle with scan rate 100 mVs^{-1} is shown in Fig. 6. Mostly, TiO_2 based working electrodes change its colour between dark blue and colorless due to the intercalation and deintercalation of ions on the film as shown in Eq. 3[17, 36]. Specifically, any cathodic peak has not been identified in all samples and a distinct anodic peak was observed at -0.6 V. It has good compliance with the previous studies for anatase structure of titania [37].

$$TiO_{2(Transparent)} + xLi^{+} + xe^{-} \leftrightarrow Li_xTiO_{2(deepblue)} \quad [3]$$

Cyclic voltammetry techniques were performed to study the recyclability of TiO_2 electrode in liquid electrolyte. They were run continuously for 500 cycles in the potential range of -2.0 V and 0.25 V with the standard Ag/AgCl reference electrode (Fig. 6). The high stability of the electrode and the liquid electrolyte was confirmed by the result obtained from the cyclic voltammetry as it cannot be seen any changes in the shape of the CV or peaks in the CV.

[Fig. 6 about here.]

Cyclability and durability of the fumed silica-based PFGE in the application of ECDs with the setout of FTO glass/TiO_2/ PFGE /FTO, were characterized by using CV. Figure 7 shows the CV performance for the first, 25th, 75th and 100th cycles. According to Fig. 7, oxidation and reduction peaks can be identified due to the existence of lithium in the PFGE. These peaks are represented chemical reactions that take place at the surface of the FTO. The drop of current up to 100 cycles was less than 1×10^{-3} A. The feature of the voltammogram changes within the first few cycles, but the shape of the cyclic voltammogram does not change sharply by cycling up to 100 cycles. The current density at the cathodic peak which corresponds to the bleaching process has gradually increased up to the 100th cycle and then decreased while the current density for the coloration process which characterizes the charge intercalation into TiO_2, increased within the first few cycles. However, there is no significant change in either shape of CV or current densities up to 100 cycles, suggesting that the device with the configuration of FTO glass/TiO_2/ PFGE /FTO glass has moderately high stability.

[Fig. 7 about here.]

3.4 SEM analysis

SEM images of LiCl, EG, and fumed silica gel electrolyte films are shown in Fig. 8 (a), (b) and (c). Spherical shape particles shown in Fig. 8a. of the PFGE belong to the fumed silica matrix and it means that the interaction of weak hydrogen bonding liquids enables to bond with the surface of the silanol group. Such bonds between particles guide to form PFGE. The uniform distribution of spherical particles can be seen in the SEM images. A large amount of dark liquid region in the micro level is accountable for the high ionic conductivity and it has further increased by a large number of liquid linkages.

According to the early studies, the increase in silica content causes a decrease of porosity [38]. The layered structure of the PFGE is shown in Fig. 8 (b) and it is confirmed the improvement of the area to

increase the conductivity. Figure 8 (c) shows the photograph of the PFGE with high concentration of pores and it causes to improvement in the ionic conductivity in PFGE. According to the uniformity, wrinkle and smooth morphology of the PFGE claims the perfect solubility of the LiCl and complete amorphous properties. Dark areas in microstructure are mainly focused liquid linkages and solvent retention potential in the PFGE. SEM images of PFGE confirm the better compatibility of LiCl, EG, and fumed silica which are used in the PFGE preparation.

[Fig. 8 about here.]

3.5 UV-Vis. Spectrum analysis

The transmittance properties of the ECD from 0–4.2 V were shown in Fig. 9 (a). The coloring effect with the voltage of the ECD is illustrated in Fig. 9 (b).

[Fig. 9 about here.]

The optical contrast (ΔT %) and the optical density (ΔOD) of the device refer to the transmittance variation and they are depended on the light absorbency of the ECD. (ΔOD) and (ΔT %) can be calculated using the relation,

$$\Delta T = T_{bleached} - T_{coloured} \quad (4)$$

$$\Delta OD_{\lambda} = Log\left[\frac{T_{bleached}}{T_{coloured}}\right] \quad (5)$$

Where, $T_{bleached}$ is the transmittance % in the de coloured state and $T_{colored}$ is the transmittance of in the coloured state.

Values of (ΔT %) and (ΔOD) with respect to the applied voltage have been calculated and tabulated as in table III. The device shows its minimum transmittance at the coloured state at around 700 nm and this implies that the intercalated Li_xTiO_2 is blue in colour as evident from Fig. 9 (b). The different colored states of the ECD were obtained with (i) decolored state by applying 0 V, (ii) an intermediate state by applying 2.0 V, and (iii) fully colored state by applying 4.2 V.

This spectro-electrochemical study further confirms the colour variation of ECDs follows Eq. 2. The optical modulation of 73% at 700 nm was observed when applying 4.2 V.

[Table 3 about here.]

Table 3
Optical contrast and optical density of the ECDs with configuration FTO glass/TiO_2/Polymer free electrolyte /FTO.

Applied voltage (V)	$T_{colored}$(%)	$T_{bleached}$(%)	ΔT%	Δ(OD)
0.0	64.558	64.558	0	0
1.0	63.819	64.558	0.739	0.005
2.0	61.511	64.558	3.047	0.02
3.0	54.696	64.558	9.862	0.072
3.5	44.766	64.558	19.792	0.16
4.0	19.722	64.558	44.836	0.51
4.2	0.568	64.558	63.990	2.0

Application on chronological amperometric double-step potential characteristics was performed (Fig. 10) to determine the stability during the sequential coloring and bleaching cycles and to calculate the response time of the devices. A double potential step between + 4.2 V and − 0.5 V was applied across the counter electrode and working electrode for cycling the prepared ECD between coloured and decoloured states. At the end of every colouring process, -0.5 V was applied and then the colouration time t_c (the time taken to reduce the light transmission through the ECD from 90–10% in the colouration process) and decouring time t_b (the time taken to intense the light transmittance through the ECD from 10–90% in the decolouring process)[39]. Under this definition, coloration and de-coloration time for the ECDs of configuration FTO/TiO_2/non-polymer electrolyte/FTO were around 42 s and 17 s respectively. The cyclic stability of the ECDs between coloring and de-coloring process was performed up to 100 cycles and it has been proven that the reversibility of the ECDs sustained even after 100 cycles.

[Fig. 10 about here.]

4. Conclusion

A novel Li^+ conducting PFGE based on fumed silica has been synthesized and characterized. Li^+ conducting liquid electrolyte has also been prepared for comparison. Relatively high ionic conductivity of 0.894 x 10^{-2} Scm^{-1} was observed for PFGE. The amorphous nature, numerous pores, and layered structure of the PFGE were confirmed by the SEM and they were liable for the high ionic conductivity in the PFGE. Studies based on cyclic voltammetric results showed the electrochemical characteristics of the reversible process and compatibility of the Li ion-based electrolyte with the TiO_2 electrode. The possibility of using the PFGE in TiO2-based ECDs has been studied. A transformable color switching between

colored and bleached states were observed when applied an appropriate voltage between two electrodes of ECD of configuration, FTO/TiO_2/ PFGE /FTO. The reversibility of the ECDs prepared with PFGE has also been confirmed.

References

1. Li W, Zhang X, Chen X, et al (2020) Effect of independently controllable electrolyte ion content on the performance of all-solid-state electrochromic devices. Chemical Engineering Journal 398:. https://doi.org/10.1016/j.cej.2020.125628
2. Li W, Zhang X, Chen X, et al (2020) Lithiation of WO3 films by evaporation method for all-solid-state electrochromic devices. Electrochim Acta 355:. https://doi.org/10.1016/j.electacta.2020.136817
3. Hadjoudis E, Mavridis IM (2004) Photochromism and thermochromism of Schiff bases in the solid state: Structural aspects. Chem Soc Rev 33:579–588. https://doi.org/10.1039/b303644h
4. Khalifa ZS (2014) Solar Energy Materials & Solar Cells Electronic structure changes of TiO 2 thin fi lms due to electrochromism. 124:186–191. https://doi.org/10.1016/j.solmat.2014.02.005
5. Mihelčič M, Šurca Vuk A, Jerman I, et al (2014) Comparison of electrochromic properties of Ni 1-x O in lithium and lithium-free aprotic electrolytes: From Ni 1-x O pigment coatings to flexible electrochromic devices. Solar Energy Materials and Solar Cells 120:116–130. https://doi.org/10.1016/j.solmat.2013.08.025
6. Weng W, Higuchi T, Suzuki M, et al (2010) A high-speed passive-matrix electrochromic display using a mesoporous TiO2 electrode with vertical porosity. Angewandte Chemie - International Edition 49:3956–3959. https://doi.org/10.1002/anie.200907008
7. Thotawatthage C, Sarangika M, Senadeera GKR, Dissanayake L (2013) Novel quasi solid state electrochromic smart windows based on TiO2 and SnO2 electrodes with PMMA gel electrolyte
8. Lin W, Zhao Q, Sun H, et al (2015) An electrochromic phosphorescent iridium(III) complex for information recording, encryption, and decryption. Adv Opt Mater 3:368–375. https://doi.org/10.1002/adom.201400396
9. Liu Q, Chen Q, Zhang Q, et al (2018) In situ electrochromic efficiency of a nickel oxide thin film: Origin of electrochemical process and electrochromic degradation. J Mater Chem C Mater 6:646–653. https://doi.org/10.1039/c7tc04696k
10. Weibin Z, Weidong W, Xueming W, et al (2013) The investigation of NbO2 and Nb2O5 electronic structure by XPS, UPS and first principles methods. Surface and Interface Analysis 45:1206–1210. https://doi.org/10.1002/sia.5253
11. Dinh NN, Oanh NTT, Long PD, et al (2003) Electrochromic properties of TiO2 anatase thin films prepared by a dipping sol-gel method. Thin Solid Films 423:70–76. https://doi.org/10.1016/S0040-6090(02)00948-3
12. Hsu CS, Chan CC, Huang HT, et al (2008) Electrochromic properties of nanocrystalline MoO3 thin films. Thin Solid Films 516:4839–4844. https://doi.org/10.1016/j.tsf.2007.09.019

13. Arvizu MA, Qu HY, Cindemir U, et al (2019) Electrochromic WO 3 thin films attain unprecedented durability by potentiostatic pretreatment. J Mater Chem A Mater 7:2908–2918. https://doi.org/10.1039/c8ta09621j
14. Sauvet K, Sauques L, Rougier A (2010) Electrochromic properties of WO3 as a single layer and in a full device: From the visible to the infrared. Journal of Physics and Chemistry of Solids 71:696–699. https://doi.org/10.1016/j.jpcs.2009.12.069
15. Li W, Zhang X, Chen X, et al (2020) Lithiation of WO3 films by evaporation method for all-solid-state electrochromic devices. Electrochim Acta 355:. https://doi.org/10.1016/j.electacta.2020.136817
16. Lee KH, Fang YK, Lee WJ, et al (2000) ž / ž / Novel electrochromic devices ECD of tungsten oxide WO thin film 3 integrated with amorphous silicon germanium photodetector for hydrogen sensor
17. Nang Dinh N, Minh Quyen N, Chung DN, et al (2011) Highly-efficient electrochromic performance of nanostructured TiO 2 films made by doctor blade technique. Solar Energy Materials and Solar Cells 95:618–623. https://doi.org/10.1016/j.solmat.2010.09.028
18. Chou J-C, Chiu Y-Y, Shih P-H, Yang S-Y (2011) Fabrication of Photoelectrochromic Cell on Flexible Substrate by Screen Printing Technique. In: The 4th IEEE International NanoElectronics Conference. pp 1–2
19. Shinde PS, Deshmukh HP, Mujawar SH, et al (2007) Spray deposited titanium oxide thin films as passive counter electrodes. Electrochim Acta 52:3114–3120. https://doi.org/10.1016/j.electacta.2006.09.053
20. Spurgeon JM, Walter MG, Zhou J, et al (2011) Electrical conductivity, ionic conductivity, optical absorption, and gas separation properties of ionically conductive polymer membranes embedded with Si microwire arrays. Energy Environ Sci 4:1772–1780. https://doi.org/10.1039/c1ee01028j
21. Gray F, Armand M (2007) Polymer Electrolytes. In: Handbook of Battery Materials. Woodhead Publishing, Great Abington, Cambridge, pp 95–160
22. Desai SS (2012) Fabrication of dual layer conducting polymer electrochromic devices using novel electrolytes. University of Wollongong
23. Jitchum V, Chivin S, Wongkasemjit S, Ishida H (2001) Synthesis of spirosilicates directly from silica and ethylene glycol/ethylene glycol derivatives. Tetrahedron 57:3997–4003. https://doi.org/10.1016/S0040-4020(01)00275-7
24. Raghavan SR, Walls HJ, Khan SA (2000) Rheology of silica dispersions in organic liquids: New evidence for solvation forces dictated by hydrogen bonding. Langmuir 16:7920–7930. https://doi.org/10.1021/la991548q
25. Yoon H, Howlett PC, Best AS, et al (2013) Fast Charge/Discharge of Li Metal Batteries Using an Ionic Liquid Electrolyte. J Electrochem Soc 160:A1629–A1637. https://doi.org/10.1149/2.022310jes
26. Ghandi K (2014) A Review of Ionic Liquids, Their Limits and Applications. Green and Sustainable Chemistry 04:44–53. https://doi.org/10.4236/gsc.2014.41008
27. Ju H, Wu J, Xu Y (2013) Revisiting the electrochemical impedance behaviour of the LiFePO 4/C cathode. Journal of Chemical Sciences 125:687–693. https://doi.org/10.1007/s12039-013-0407-9

28. Di Noto V, Longo D, Münchow V (1999) Ion-oligomer interactions in poly(ethylene glycol)400/(LiCl)x electrolyte complexes. Journal of Physical Chemistry B 103:2636–2646. https://doi.org/10.1021/jp983764y
29. Krishnan K, Krishnan RS (1966) Raman and infrared spectra of ethylene glycol. Proceedings of the Indian Academy of Sciences - Section A 64:111–122. https://doi.org/10.1007/BF03047675
30. Pucić I, Jurkin T (2012) FTIR assessment of poly(ethylene oxide) irradiated in solid state, melt and aqeuous solution. Radiation Physics and Chemistry 81:1426–1429. https://doi.org/10.1016/j.radphyschem.2011.12.005
31. Vasudevan V, Wang M, Yuwono JA, et al (2019) Ion Agglomeration and Transport in MgCl2-Based Electrolytes for Rechargeable Magnesium Batteries. Journal of Physical Chemistry Letters 10:7856–7862. https://doi.org/10.1021/acs.jpclett.9b03023
32. Aziz SB, Brza MA, Hamsan MH, et al (2020) Effect of ohmic-drop on electrochemical performance of EDLC fabricated from PVA:dextran:NH4I based polymer blend electrolytes. Journal of Materials Research and Technology 9:3734–3745. https://doi.org/10.1016/j.jmrt.2020.01.110
33. Perumal P, Abhilash KP, P.Sivaraj, Selvin PC (2019) Study on Mg-ion conducting solid biopolymer electrolytes based on tamarind seed polysaccharide for magnesium ion batteries. Mater Res Bull 118:. https://doi.org/10.1016/j.materresbull.2019.05.015
34. Capeletti LB, Zimnoch JH (2016) Fourier Transform Infrared and Raman Characterization of Silica-Based Materials. Applications of Molecular Spectroscopy to Current Research in the Chemical and Biological Sciences 3–22. https://doi.org/10.5772/64477
35. Seo D, Park J, Shin TJ, et al (2015) Bathochromic shift in absorption spectra of conjugated polymer nanoparticles with displacement along backbones. Macromol Res 23:574–577. https://doi.org/10.1007/s13233-015-3078-1
36. Scrosati B (1993) Laminated electro chromic displays and windows
37. Jourdani R, Outzourhit A, Oueriagli A, et al (2004) Active and Passive Electronic Components. 27:125–131
38. He X, Shi Q, Zhou X, et al (2005) In situ composite of nano SiO 2 – P (VDF-HFP) porous polymer electrolytes for Li-ion batteries. 51:1069–1075. https://doi.org/10.1016/j.electacta.2005.05.048
39. Sarangika HNM, Dissanayake MAKL, Senadeera GKR, Karunarathne WGMD (2019) Materials Today : Proceedings Low cost quasi solid state electrochromic devices based on F-doped tin oxide and TiO 2. Mater Today Proc. https://doi.org/10.1016/j.matpr.2019.07.585

Figures

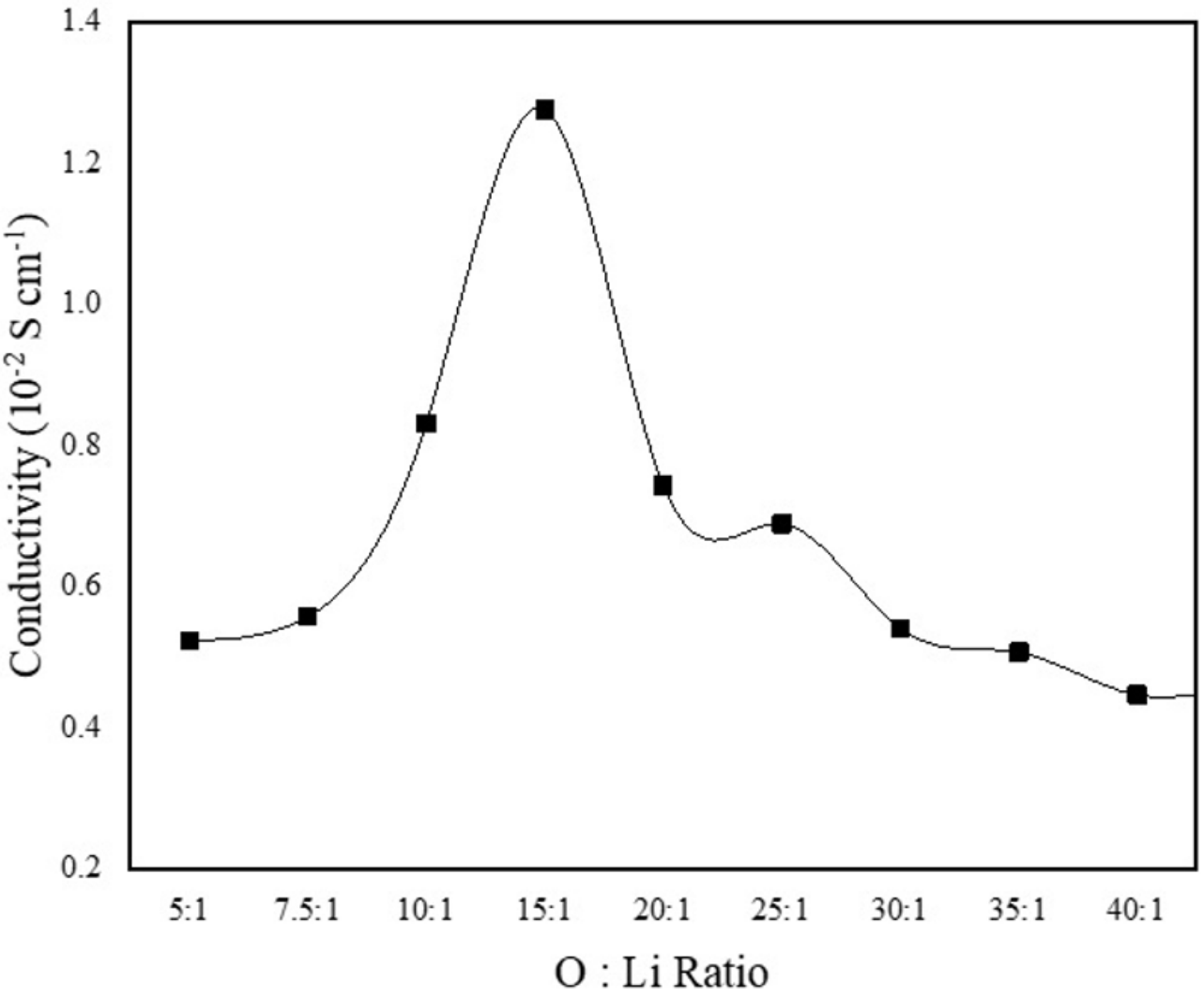

Figure 1

Figure 1

Room temperature Ionic conductivity of the liquid electrolytes at different (O: Li+) ratio

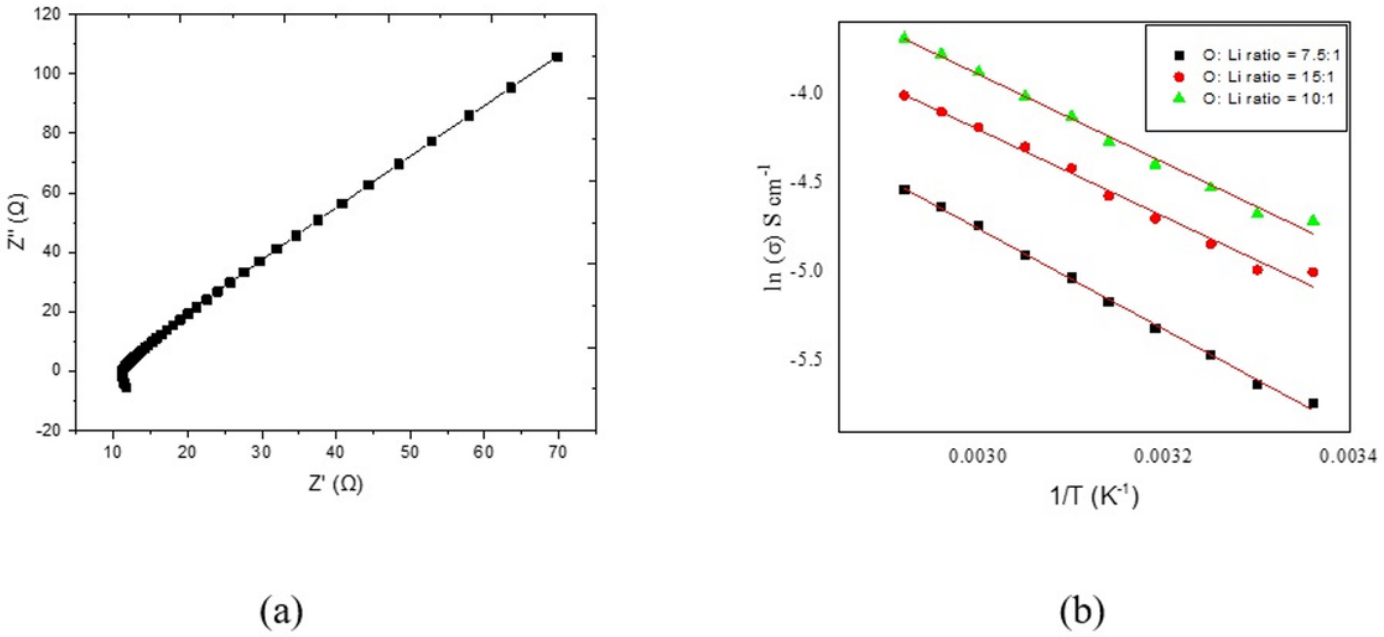

Figure 2

Figure 2

(a) Nyquist plot for the polymer free gel electrolyte of O: Li^+ =10:1 at room temperature. (b) variation of the ionic conductivities of polymer free gel electrolyte with temperature.

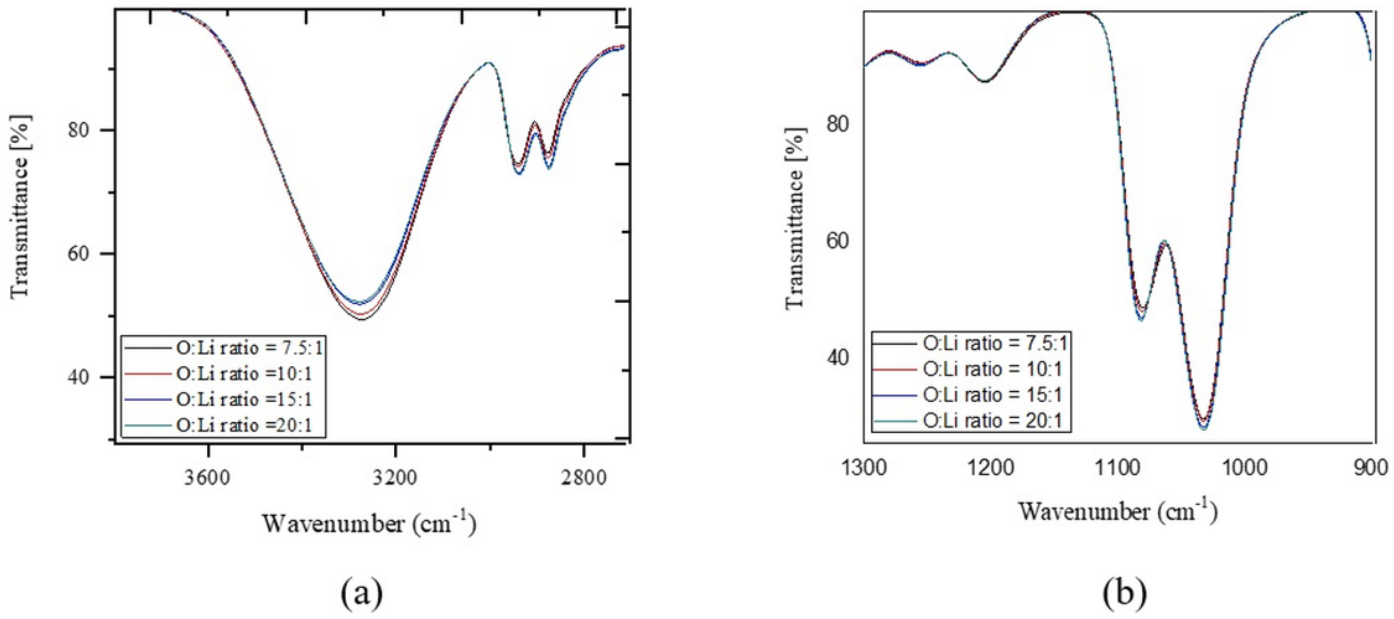

Figure 3

Figure 3

a) intensity variations of O-H stretching vibrations with Li ion concentration 2.b). Intensity variations of .C-O stretching vibrations with Li ion concentration at 1080 cm^{-1}.

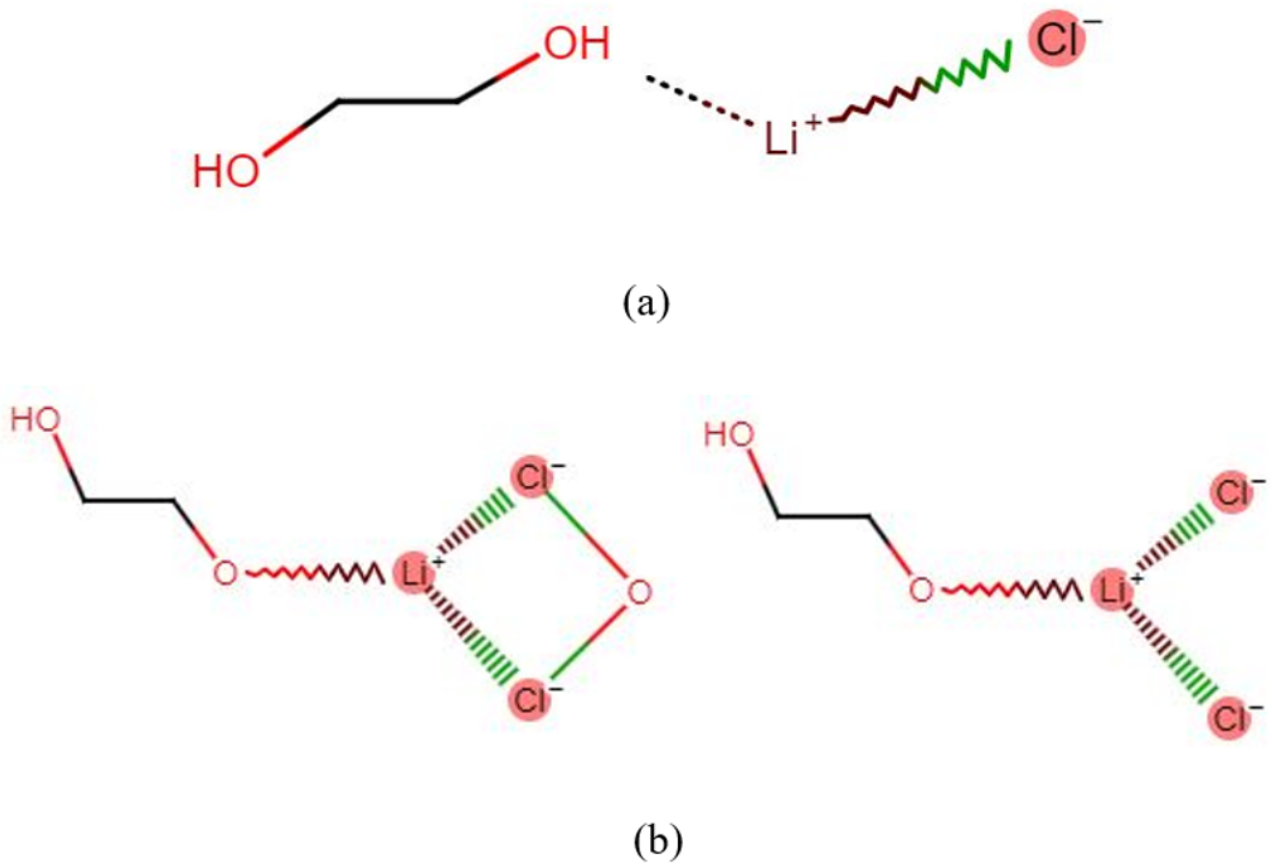

Figure 4

Figure 4

Possible ion pair and aggregates assisted to sudden decrease of the ionic conductivity, (a) Ion pair, (b). Possible aggregates

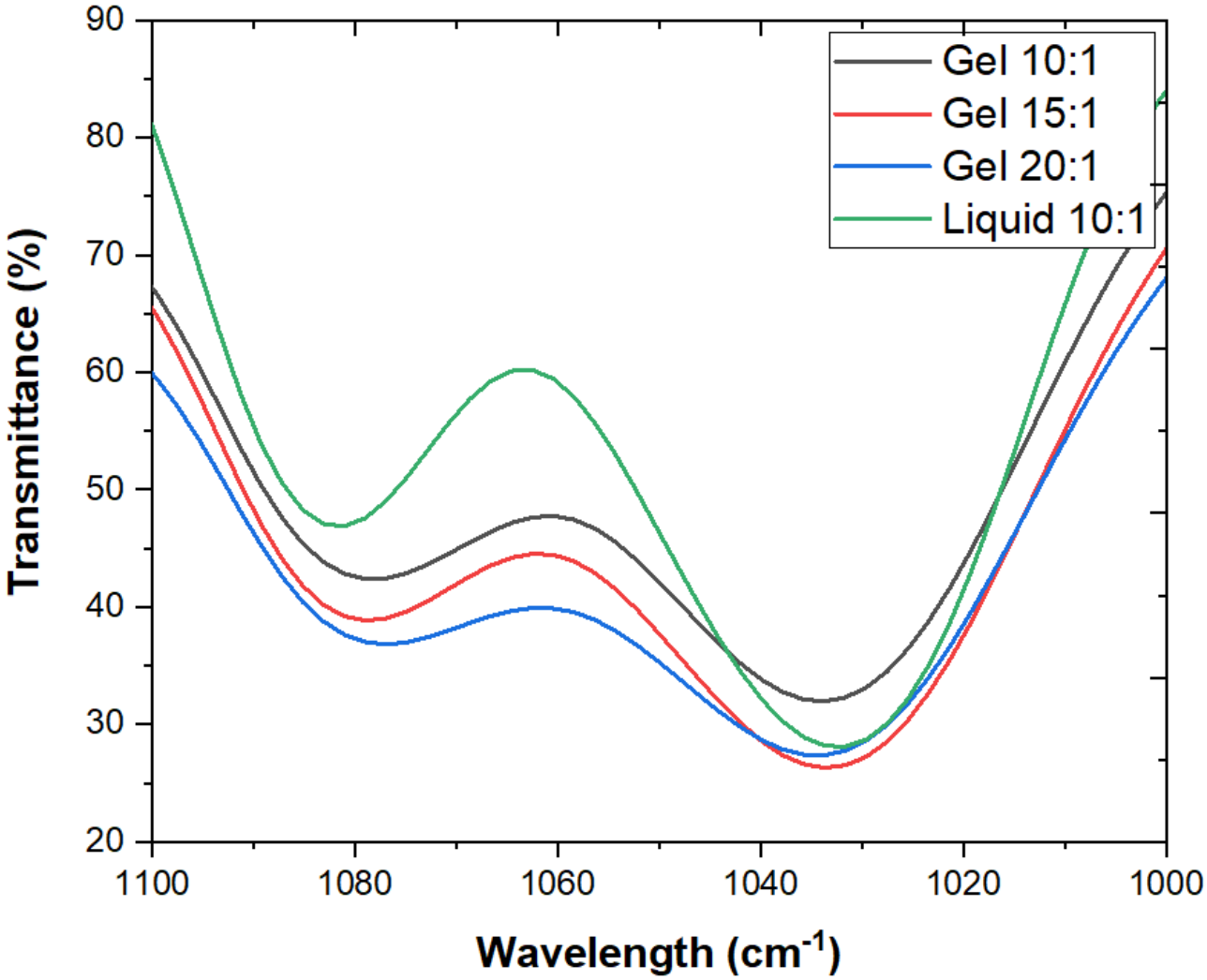

Figure 5

Figure 5

The FTIR Peak shift at 1081 cm^{-1} with the Li-ion concentration of polymer free gel electrolytes.

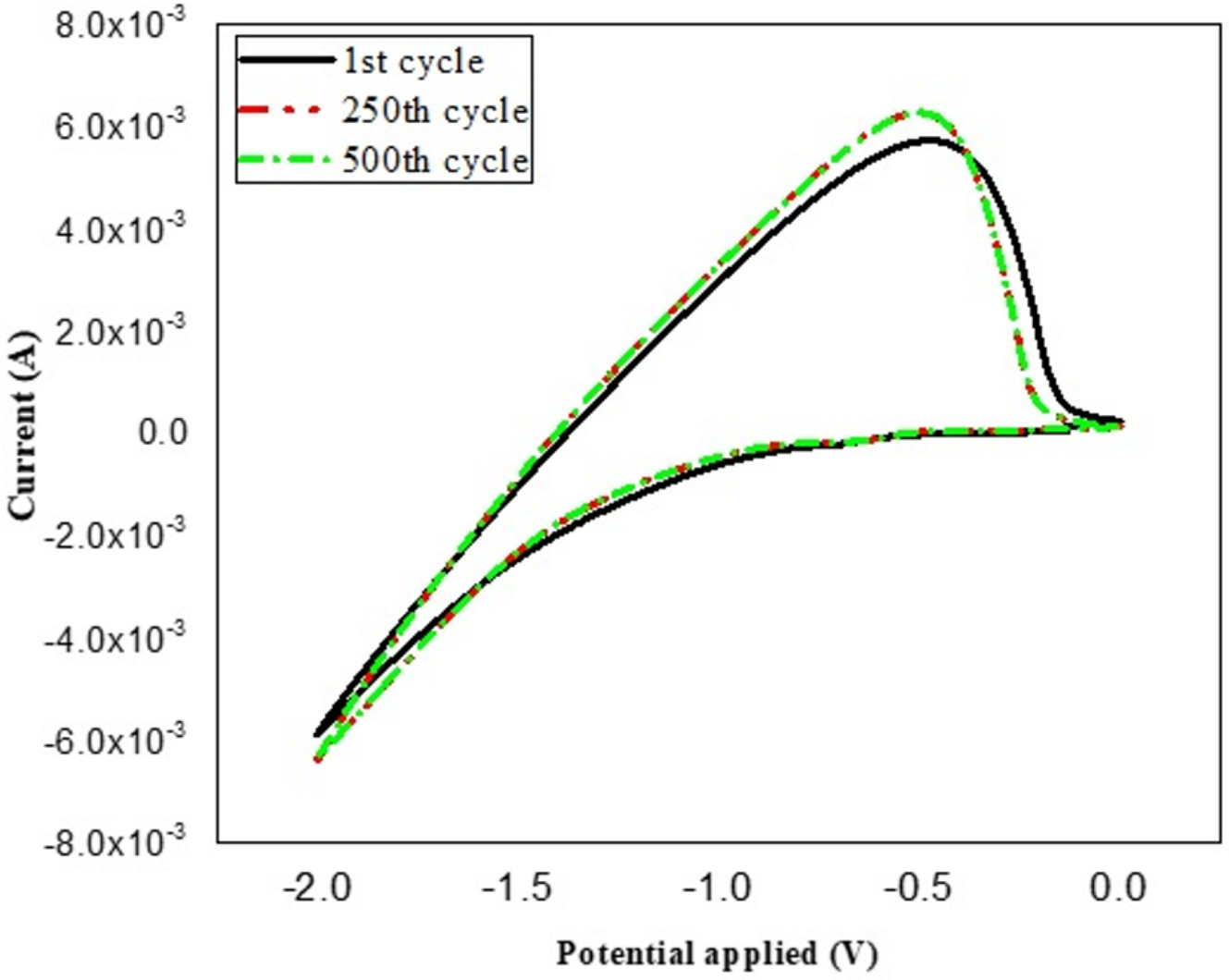

Figure 6

Figure 6

Cyclic voltammetry of TiO_2/FTO in EG/ LiCl liquid electrolyte (O: Li^+ = 15:1) molar ratio from 1- 500 th cycle with scan rate 100 mVs^{-1}.

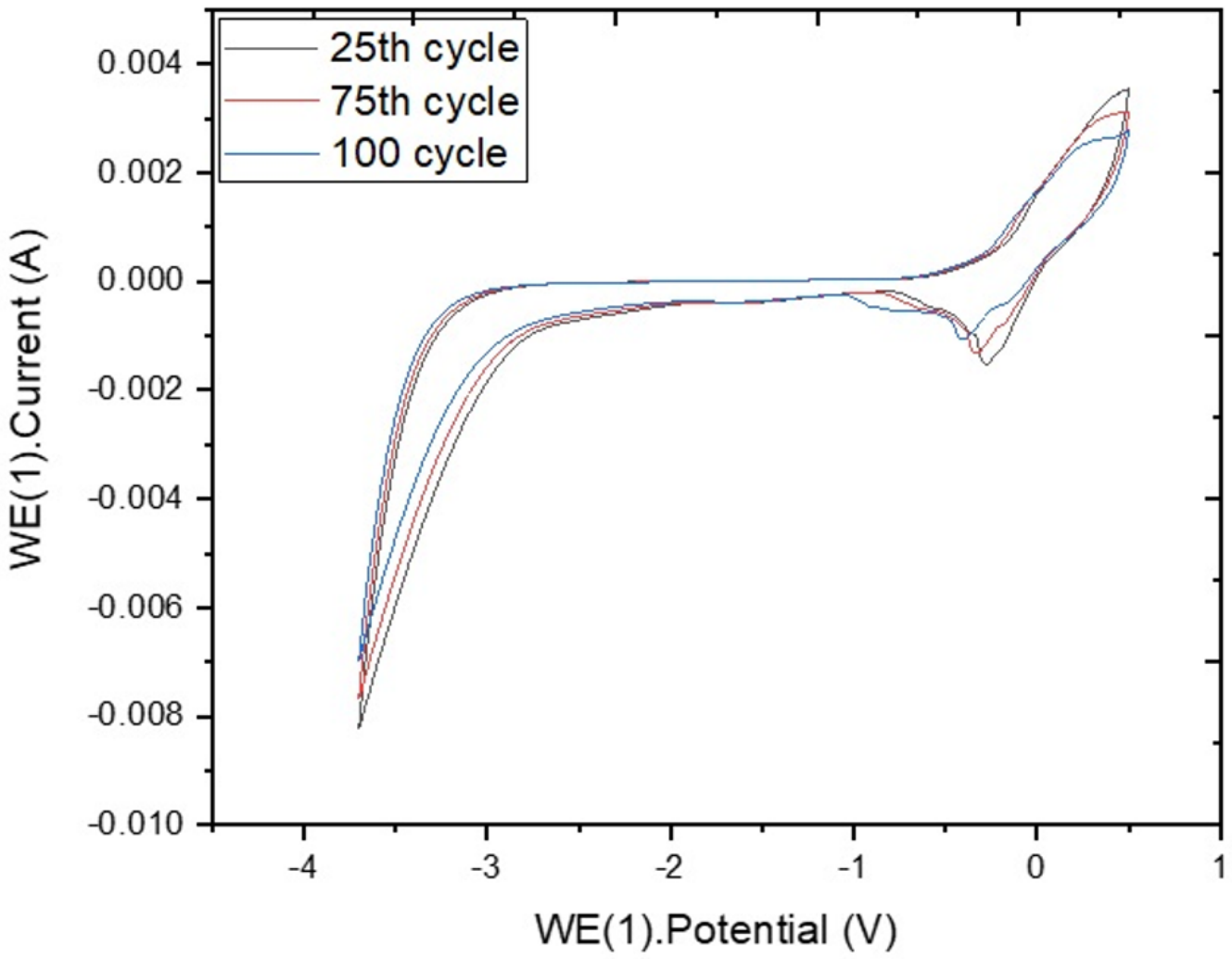

Figure 7

Figure 7

Cyclic voltammograms for an ECD with the configuration FTO/TiO_2/non-polymer electrolyte/FTO for the 25^{st}, 75^{th}, and 100^{th} cycles. Scan rate 100 mVs^{-1}.

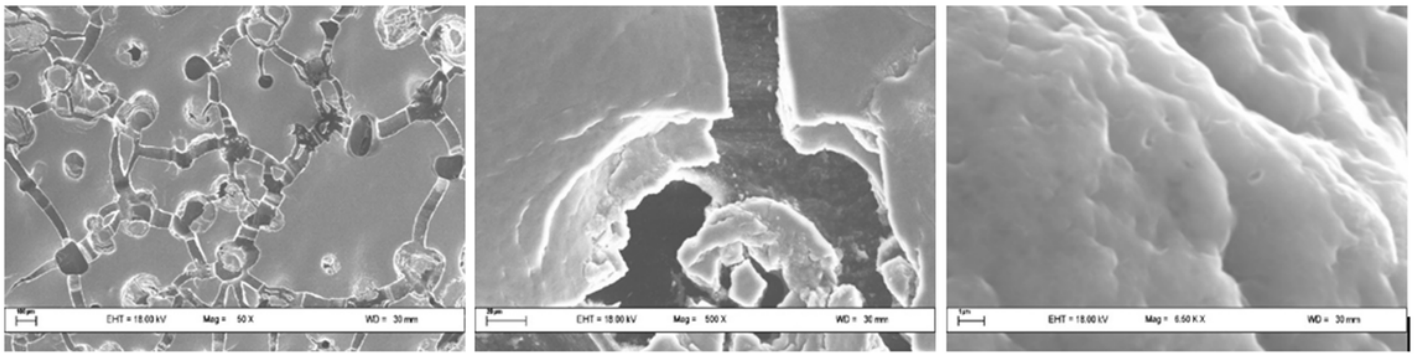

(a) (b) (c)

Figure 8

Figure 8

SEM image of the electrolyte LiCl/EG/Fumed silica, (a). 50 x magnification (b). 500 x magnification (c). 6.5 k x magnification.

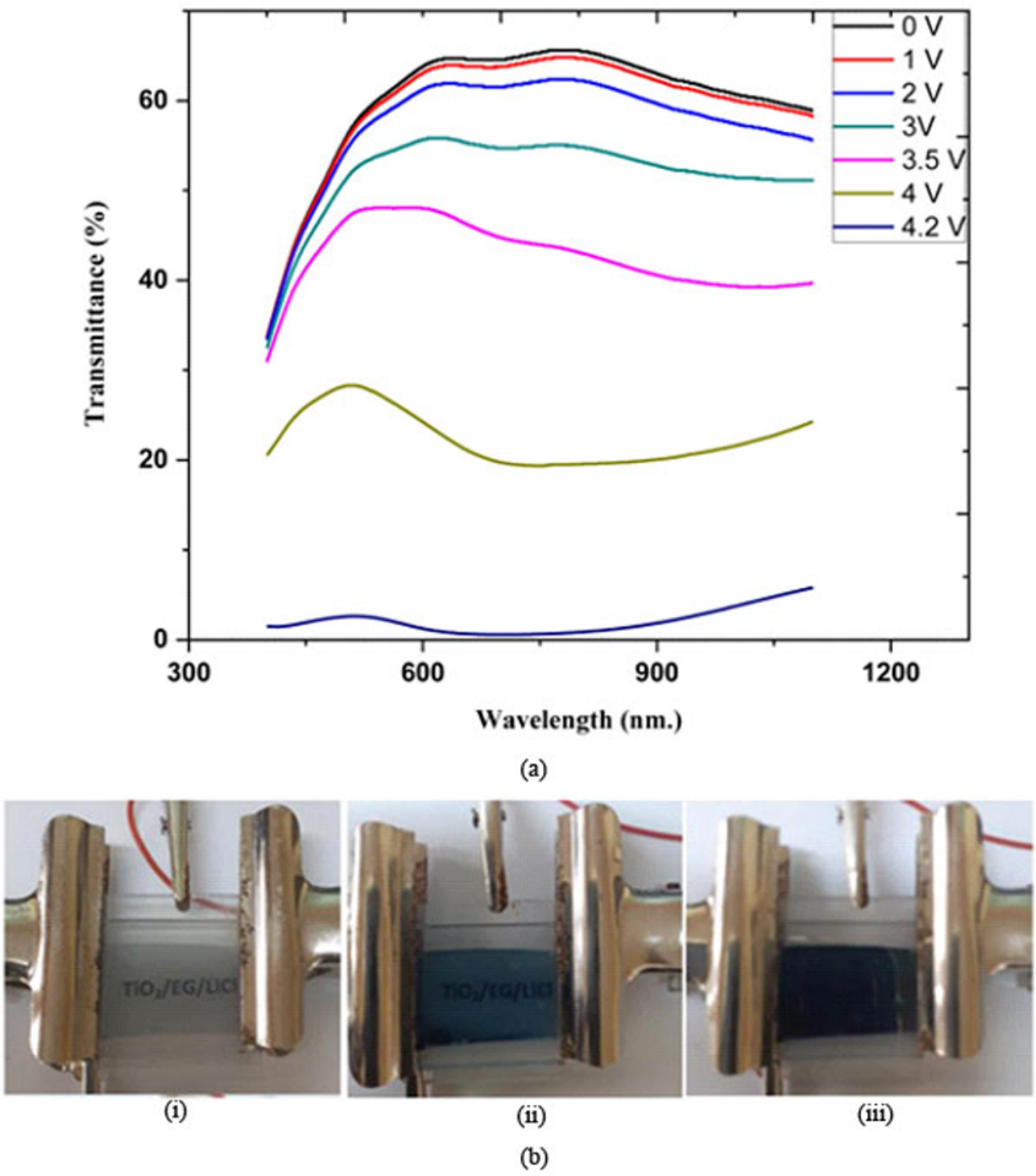

Figure 9

Figure 9

(a) Optical transmittance as a function of wavelength for the electrochromic devices FTO/TiO_2/non polymer electrolyte/FTO in various potential stages (b) Different electrochemical statues of the device FTO/TiO_2/non-polymer electrolyte/FTO (i) as prepared (ii) colored (partially reduced) (iii) highly reduced.

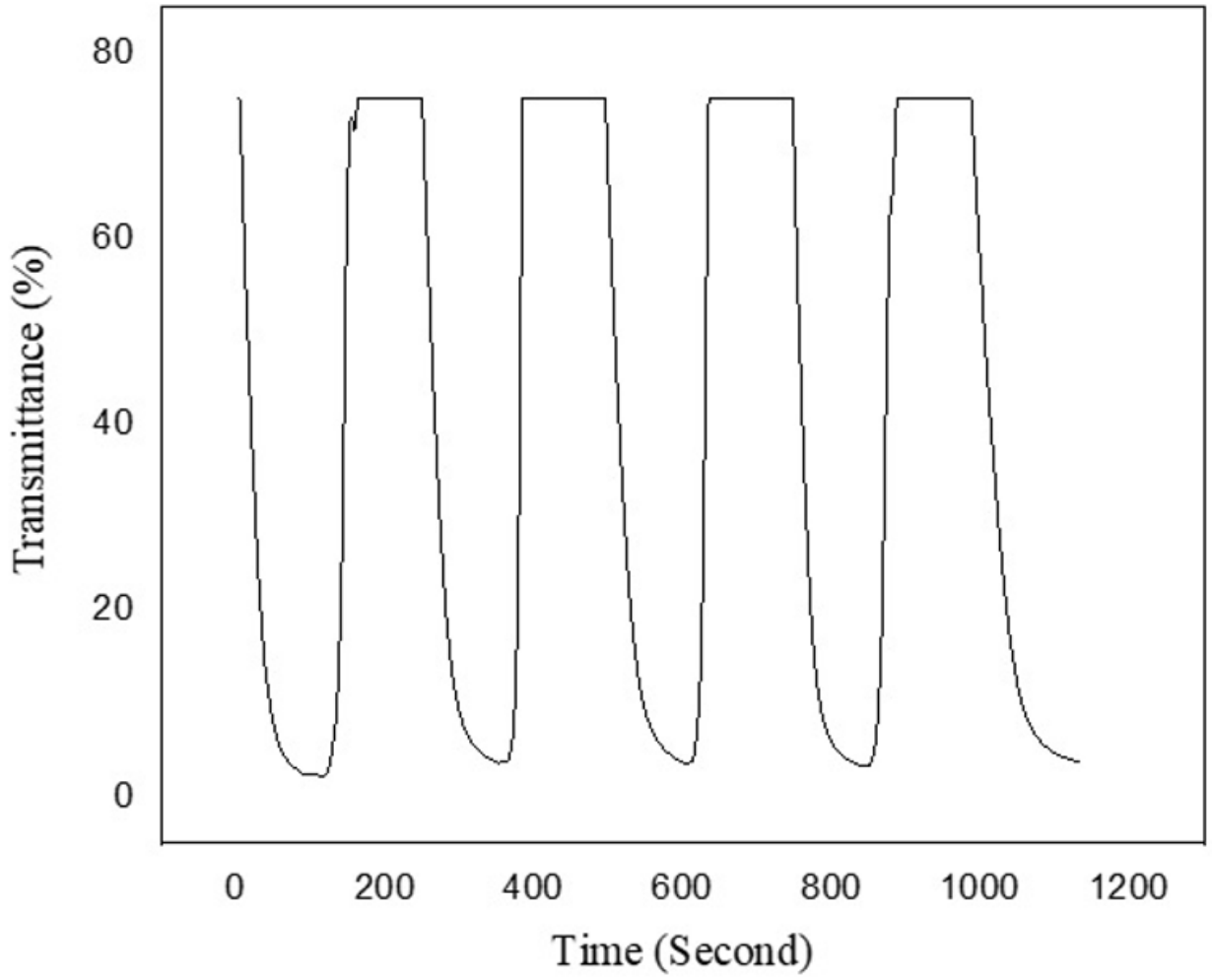

Figure 10

Figure 10

Reversibility of the ECD applying -0.5 and 4.2 V with configuration FTO/TiO_2/non-polymer electrolyte/FTO.

Supplementary Files

This is a list of supplementary files associated with this preprint. Click to download.

- GraphicalabstractFinal.png